Journal of ASTM International, Vol. 3, No. 9
Paper ID JAI100374
Available online at www.astm.org

K. E. Perry,[1] *P. E. Labossiere,*[1] *and E. Steffler*[2]

Thermoelastic Transformation Behavior of Nitinol

ABSTRACT: The transformation behavior of Nitinol under uniaxial tension and four-point bending was investigated. A novel sample geometry produced from drawn tubing was used to observe the differences caused by localized phase transformation effects between the two types of loading and between samples with different process and load histories. Phase shifted moiré interferometry was used to provide full-field measurement of strain during the experiments. Optical resolution and grating coherence were sufficient to simultaneously resolve the strain fields within both the parent and transformed phases of the material. Evidence of both localized and uniformly distributed phase transformation is observed for the samples tested in tension while the bending results clearly indicate an asymmetric neutral axis and a complex reverse bending response for samples containing a strong R-phase component and tested at temperatures below critical transformation temperatures.

KEYWORDS: Nitinol, thermoelasticity, phase transformations, photomechanics, moiré interferometry, full-field measurements, modeling, carrier fringes

Introduction

Nitinol has seen increased use in medical applications where devices are compressed to catheter dimensions, delivered through tortuous anatomy, and deployed in various diseased locations within the human body. The material is well suited to the design constraints imposed by such conditions and often provides incomparable advantages over other engineering materials. Alloy composition and processing history can [1–3] be used to achieve a broad range of material response that can be tailed to intended applications.

The stress-induced phase transformation and mechanical behavior of Nitinol have been generally described [4] and progress has been made on many fronts to further understanding of shape memory and superelastic material behavior [5–7]. Accurate and reliable measurements of material properties in Nitinol are difficult due to the material's strong dependence on temperature, processing, and load history as well as the phase transformation behavior that may exhibit localization. Global measurements, such as strain obtained using an extensometer during uniaxial tensile testing, can obscure the effect of localized transformation bands and potentially mislead interpretations of material behavior.

The interferometric measurement technique of moiré interferometry [8] is an excellent candidate for providing accurate material property information in Nitinol. The technique is well established and is routinely used to characterize complex material behavior playing a pivotal role in the development and validation of constitutive models for advanced engineering materials [9].

Recent studies by the authors have demonstrated the applicability of phase shifted moiré interferometry to strain measurements in Nitinol [10] with special attention to experimental details such as the effect of specimen grating thickness and density, fringe analysis, and the quantification of full-field strains [11].

Presently we utilize a novel sample design to measure full-field strain during uniaxial tension and four-point bending of Nitinol. Differences caused by localized phase transformation effects were studied in detail through the use of carrier fringes with samples having different process and load histories. Here we present only key results showing the capabilities of phase shifted moiré interferometry, the difficulties associated with Nitinol calibration due to the complex transformation behavior, and the sensitivity of the material to temperature. The results presented herein are not complete and are merely representative results of numerous experiments still underway in our laboratory.

Manuscript received December 5, 2005; accepted for publication April 14, 2006; published online October 2006. Presented at ASTM Symposium on Fatigue and Fracture of Medical Metallic Materials and Devices on 7–11 November 2005 in Dallas, TX; M. R. Mitchell and K. Jerina, Guest Editors.

[1] ECHOBIO LLC, 579 Azalea Avenue, Bainbridge Island, WA98110.
[2] Idaho National Engineering Laboratory, Idaho Falls, ID83415.

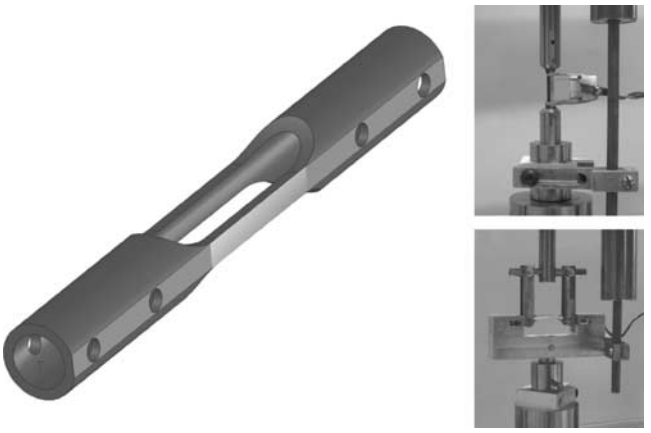

FIG. 1—*Schematic of the test sample and photographs of the tensile and four-point bend configurations.*

Test Samples

Material and Processing History

The material used in this study was SE-508, seamless drawn tubing from Nitinol Devices and Components, Inc., with an as-received A_f of −9 °C. Two distinct heat treatments were chosen, denoted by A and B. Treatment A was performed at 325 °C for 60 min and Treatment B was performed at 500 °C for 30 min. All samples were water quenched subsequent to heat treating.

The active A_f temperatures were measured for all test samples following ASTM standard F 2082 for free bend and recovery over the temperature range from −30 to 30 °C. Very consistent results were obtained and representative curves of deflection versus temperature are shown in Figs. 3 and 4 for the two heat treatments. Treatment A resulted in test samples with an active A_f of 25.4 °C and exhibited a strong R-phase component with an R'_f of −3.5 °C. Treatment B did not exhibit a noticeable R-phase component and had an active A_f of 22 °C.

Geometry and Loading

A single sample geometry was chosen for both uniaxial tension and four-point bending tests. Figure 1 is a schematic of the sample geometry and photographs of the two loading scenarios.

Two pairs of holes were laser cut in the ends of the samples and then carefully honed to ensure precision pin loading of the test samples. The gage section of the samples were EDM'ed to produce perpendicular edges, maximizing the amount of material in the gage section and ensuring uniform behavior in bending. Slow feed, low power, and multiple passes were used to minimize adverse effects on the

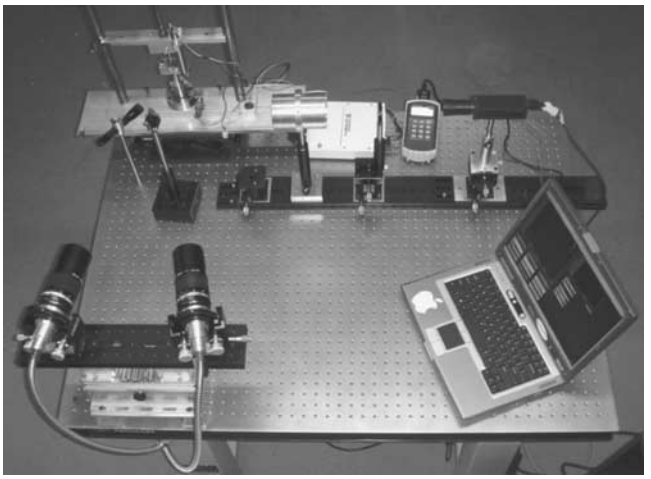

FIG. 2—*Photograph of the custom load frame in the moiré interferometer.*

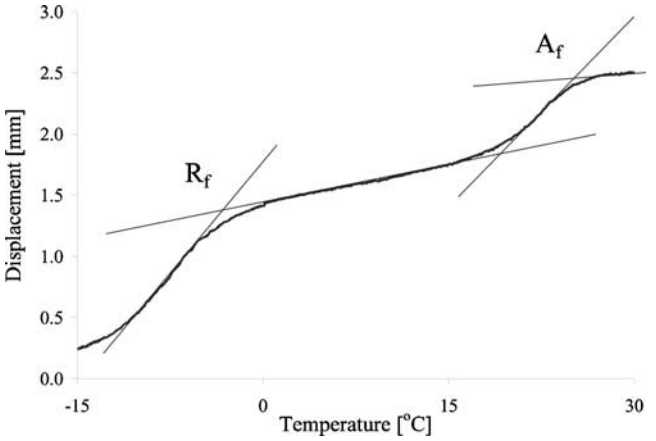

FIG. 3—*Displacement versus temperature from the free bend recovery test for material A showing location of A_f and R_f.*

bulk material properties. A flat surface was carefully ground on one face of the test samples to provide an optically flat surface for the grating replication process. Prior to production of the samples, FEA was used to optimize the design of the sample geometry and the corresponding fixtures to achieve uniform tension and pure bending over a large range of deformations. A slow loading rate (<1 mm/min) was used for all of the tests.

Testing

Global Measurements

Global (far-field) measurements of the sample load, extension, and displacement were made using a load cell, extensometer with a gage length of 10 mm and LVDT, respectively. Additionally, thermocouples were used to monitor the ambient temperature and the sample temperature throughout the experiments. Prior to beginning an experiment, the temperature was raised well above A_f and then slowly lowered to the desired test temperature to ensure an initial fully austenitic state. Ambient test temperatures were held constant within 1 °C throughout all of the experiments.

The samples were loaded in either tension or bending using a custom-built load frame and fixtures. Figure 2 shows a photograph of the load frame with a sample mounted in the moiré interferometer and imaging system. The experiments employed two personal computers, one each for the data acquisition and

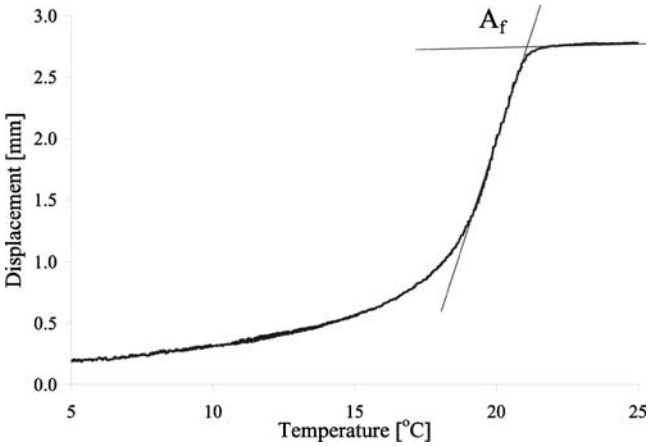

FIG. 4—*Displacement versus temperature from the free bend recovery test for material B showing location at A_f.*

imaging systems. Load, deflection, and extension measurements were digitized to 16 bits and recorded using a conventional data acquisition system at 50 Hz. Calibration for all sensors was performed to ensure accurate measurements.

Full-field Measurements

Moiré interferometry is a well established method in experimental mechanics and has been applied to single crystal shape memory materials [12]. The general technique is described in detail in [8]. For our work, we exploit phase shifting [13] that provides exceptional noise reduction while enhancing spatial resolution. Five phase shifted images were recorded for each full-field measurement at a resolution of 1280 by 960 pixels with 10 bit grayscale resolution. The typical field of view was on the order of 1–2 mm.

The interferometer used for these experiments was custom built with an integrated fiber optic splitter and phase shifter to provide exceptional stability and configurability [14]. Diffraction gratings were produced from holographic exposures of photographic plates. They were epoxy replicated using a method capable of producing a final grating thickness of 5–20 μm. A grating density of 300 L/mm was chosen to maximize measurement sensitivity for the anticipated range of deformations. This resulted in a fringe order sensitivity of 1.67 μm/fringe.

Carrier fringes [8] were used to extend the range over which displacement measurements could be made. Carrier fringes are produced by changing the angles of the incident beams and provide an offset to the effective diffraction grating density. They do not increase or decrease the inherent sensitivity of moiré interferometry data, but rather change the number of fringes produced for a given deformation. By dialing in or out carrier fringes, an extended measurement range was achieved so that strain measurements could be made in both the austenite and martensite phases.

Fringe analysis was performed manually by plotting the wrapped fringe contours and counting them edge to edge. The phase shifted data provided excellent contrast for identifying fringe centers as well as resolving the slope of the wave front. The gage length used for strain calculations was kept consistent for any given series of measurements, and was usually on the order of 0.5–0.8 mm (toward the higher end of the range for the tensile measurements and the lower end of this range for the bend measurements). The choice of gage length for the full-field measurements had little significance in the strain measurements over this range for both the tensile and bend tests. The estimated precision of the strain measurements was determined to be ±0.02 %.

Tension Test Results

Figure 5 shows a sequence of images of wrapped fringes of the tensile loading for a representative sample processed according to Treatment B. The sample was tested at a temperature of 19 °C which is below the active A_f temperature of the material. Figures 5(*a*)–5(*h*) show a sequence of images during the tensile loading portion. Transformation occurs at both the top and bottom of the gage section as the loading increases and propagates towards the middle of the sample. Figure 5(*i*) shows an optically magnified view of the upper transformation region boundary. Figures 5(*j*) and 5(*k*) are for an intermediate unloading and full unloading, respectively. Lastly, Fig. 5(*l*) shows the image for full unloading but with the carrier removed.

Figure 6 shows the stress versus strain behavior using both the global measurements denoted by the solid line and the full-field measurements denoted by the open circles and connected by the dashed line. Note that the full-field results show that the local strain is either in the 0 to 1% range or in the 3.5–5% range in the austenite and martensite, respectively. Strains between these two appear only in the global measurements. Measurements of parent phase and transformation zone dimensions along with the measured strain values for each were used to compute an effective global strain estimate. The results of these calculations agreed exceptionally well with the measured global strain measurement.

Figure 7 shows a sequence of images of wrapped fringes of the tensile unloading for a representative sample processed according to Treatment A. Here the material was tested at a temperature below the active A_f temperature (22 °C) but well above the R_f temperature. Figure 8 shows the stress versus strain behavior using both the global measurements denoted by the solid line and the full-field measurements denoted by the open circles and connected by the dashed line.

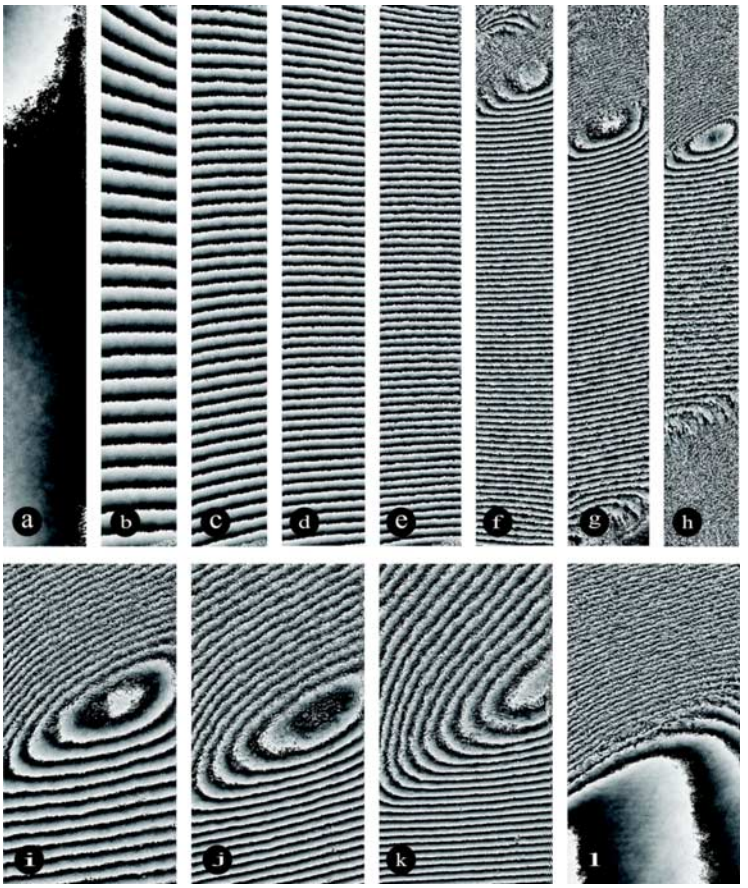

FIG. 5—*Sequence of images of unwrapped fringes during the tensile loading and close-up of unloading of material B.*

Bend Test Results

Figure 9 shows a sequence of images of wrapped fringes of the four-point bending for a representative sample processed according to Treatment A. Figures 9(*a*)–9(*c*) are for increasing load. Figure 9(*d*) is for nearing full unloading. Figures 9(*e*)–9(*h*) are for load reversal and up to nearing full unloading. The images clearly show that there is asymmetry in the tensile and compressive behavior material which is reflected in the off-center location of the neutral axis. Analysis of the fringe patterns clearly showed that the strain varied linearly through the cross section of the beam for both material treatments and all test temperatures investigated.

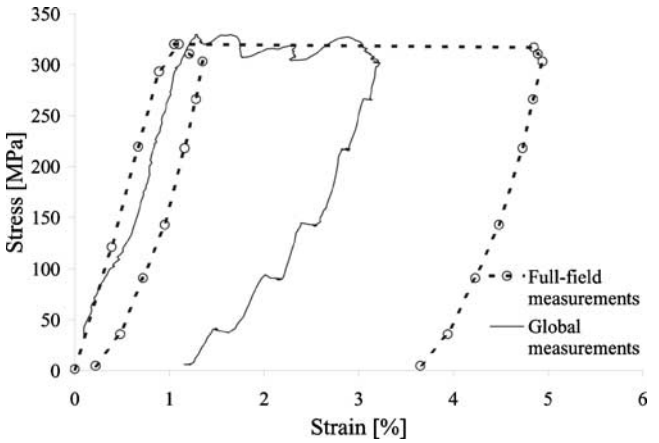

FIG. 6—*Stress versus strain behavior for material B using both the global and full-field measurements.*

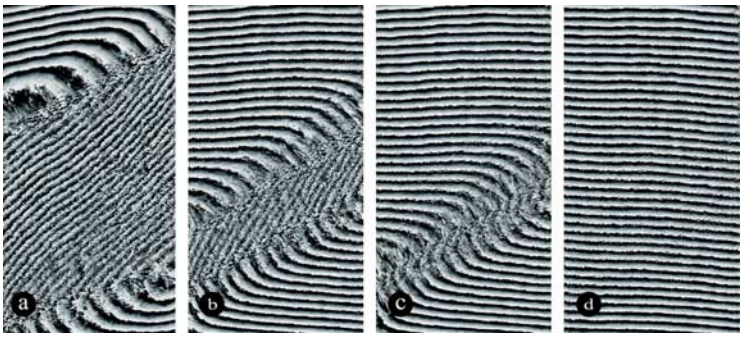

FIG. 7—*Sequence of images of unwrapped fringes during the tensile unloading of material B showing the disappearance of the transformation zone.*

Figures 10 and 11 shows the global load versus full-field strain measurements at the top and bottom edges of the sample during loading and reverse loading under four-point bend for representative samples processed according to Treatments A and B, respectively. In both cases the strains on the tensile side were higher than the strains on the compressive side of the specimen.

Reverse loading for a representative sample processed according to Treatment A showed a clear difference in measured response presumably indicating the influence of the strong R-phase component present in this material. The sample processed according to Treatment B and tested under four-point bending showed no residual strain since unlike the tensile test results presented for this treatment, this test was performed at 24 °C that is above the A_f temperature of this treatment.

In both the forward and reverse loading of the sample treated according to Treatment B and the forward loading of the sample treated according to Treatment A, the ratio of the measured strains on the top edge and the bottom edge of the sample remained constant. This ratio was larger for the case of the sample treated according to Treatment B.

Discussion

The Utility of the Full-field Measurements

The technique of phase shifted moiré is shown here to provide accurate and reliable measurements of strain in both the parent and transformed phases of Nitinol under tensile and four-point bending with large deformations. The utility of such measurement results depends on the available measurement range and sensitivity of the measurement system which in turn depends directly on the quality of the fringe patterns.

Grating Quality—The quality of a fringe pattern is strongly affected by the performance of the diffraction grating. Diffraction gratings used for moiré interferometry must be efficient diffractors, espe-

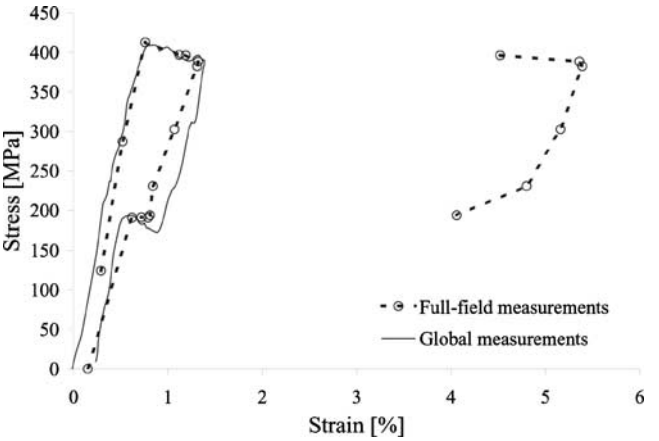

FIG. 8—*Stress versus strain behavior for material A using both the global and full-field measurements.*

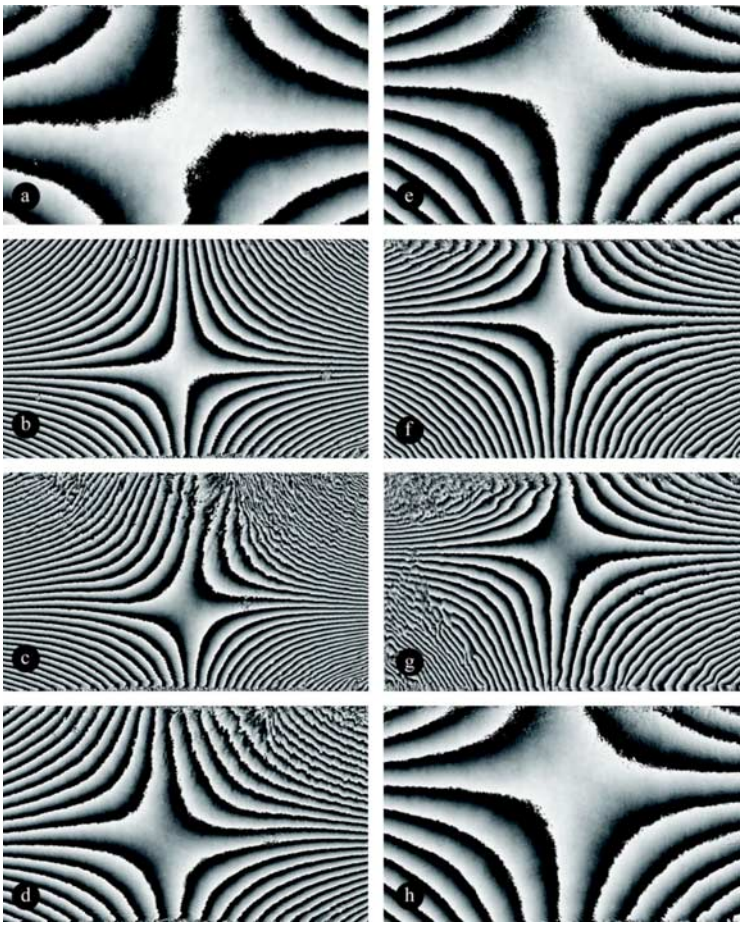

FIG. 9—*Sequence of images of unwrapped fringes during loading, unloading and reverse loading under four-point bending of material A.*

cially in the ±1 diffraction orders and they must be excellent reflectors. The gratings also must be adequately thin to minimize shear lag [8] and to not obscure fine spatial detail. Very thin (zero-thickness) photoresist gratings exposed in situ have been shown to clearly reveal edges and other microstructural details in Nitinol [11,15], but are difficult to pattern over large areas and tend to have higher background noise than replicated gratings.

Alternatively, thin epoxy replicated gratings were used in this work to provide an exceptional optical signal at the expense of slightly obscured spatial detail. This was an acceptable trade-off as the strain measurements of concern were made over significantly larger gage lengths than would be affected by the

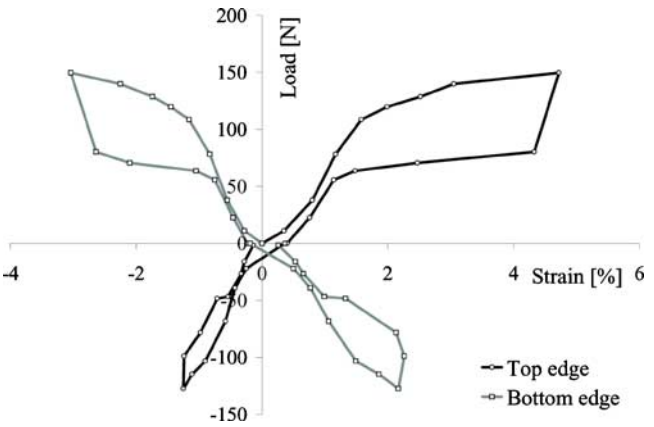

FIG. 10—*Global load versus full-field strain measurements at the top and bottom edges of the sample during loading and reverse loading under four-point bend for material A.*

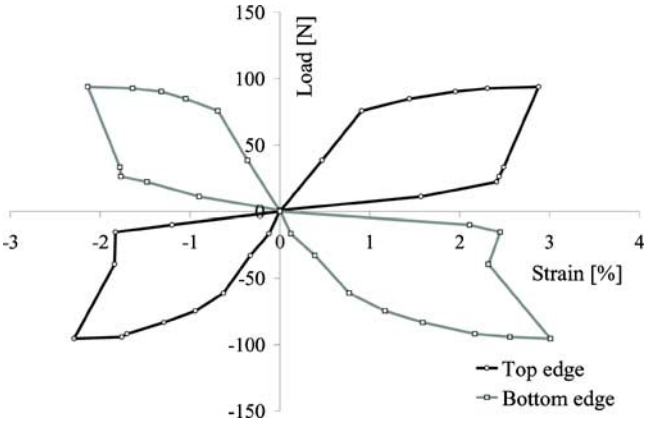

FIG. 11—*Global load versus full-field strain measurements at the top and bottom edges of the sample during loading and reverse loading under four-point bend for material B.*

thickness of the grating. Nonetheless, the thin epoxy gratings used for this work did exhibit shear lag effects most notably as viscoelastic relaxations of the grating (lasting on the order of seconds) after abrupt load changes.

Specimen reflectivity is directly affected by large deformations and the transformation process. The gratings used in this work proved extremely rugged and did not show any degradation in signal quality for the relatively small number of loading cycles considered, even while the physical appearance of the gratings was affected even after a single loading cycle producing localized phase transformation.

Carrier Fringes—Not unlike other full-field strain measurement techniques such as digital image correlation or speckle interferometry to name a few, there is an inherent trade-off between sensitivity and measurement range with the technique of moiré interferometry. Too much sensitivity results in more fringes than can be resolved with a digital acquisition system (a requirement for phase shifting) and too little resolution obviously reduces the precision of the displacement and strain measurements.

For these experiments the technique of carrier fringes was used to increase the range over which phase shifted measurements could be made while preserving the use of a high density grating. Carrier fringes do not add any additional optical information, they simply provide more or less fringe centers on which measurements are based [8].

Various methods for introducing the carrier fringes and for validating the measurements produced by this method were explored. The method chosen for these experiments was confirmed to produce a repeatability better than 0.02 % strain. Slight modifications of the interferometer were required to maintain optimal beam coverage over the large range of optical system adjustment required for the measurements presented herein. Phase shifting proved particularly helpful in analysis of the carrier frequency fringe patterns as it clearly distinguishes the sign of the optical wave front.

The Importance of Test Sample Design

Specimens Cut from Tubes—Fabrication of the test samples from seamless drawn tubing was chosen because of the importance of tubing to medical device applications and because processing is known to affect texture and, hence, the properties of Nitinol. As described in [16], equivalent thermomechanical processing can be used to reproduce the desired material response from samples scaled to different physical dimensions. By utilizing samples produced from tubing, we have demonstrated a technique that has great utility for medical devices and their applications.

Effect of Loading Configuration—The design of a single sample geometry capable of being tested in both simple uniaxial tension and pure four-point bending enabled us to explore differences between alternative loading configurations with a high degree of consistency.

Previous moiré interferometry results [11] have already demonstrated the effects of localization in the production of Lüders-type bands in uniaxial tension. Our current results have now confirmed that local-

ization also occurs in samples tested under four-point bending. The degree and uniformity of the localization is markedly different from that produced in tension, most likely a result of the more controlled strain state produced in bending.

Furthermore, for the representative sample processed according to Treatment A, noticeable nonrecovered strain was evident after the forward loading cycle and prior to reverse loading. Although not apparent in the global tensile test results, the effect of this was clearly evident in the plot of full-field strain for this sample in bending (Fig. 10).

Observation of Trends for the Different Processing Histories

The samples treated according to Treatment A required higher loads to induce transformation than the samples treated according to Treatment B. They also appeared stiffer in loading and exhibited more dramatic localization effects. Although not directly apparent in the global test results, the presence of the R-phase contributed significantly to the difference observed in the transformation strain behavior of the two treatments.

Conclusions

Measurements of strain were made simultaneously in both the parent and transformed phases of Nitinol for two distinct loading configurations. Comparisons were made to global measurements of strain to highlight the need for the correct interpretation and use of such measurements for calibrating material models describing Nitinol.

The strain data presented for the two material heat treatments were congruent with the bend free recovery data when the test temperatures are taken into consideration. For Treatment A, both tensile and bend tests were performed at the same temperature (22°C) that was slightly below the material's A_f of 25.4°C. Only a small residual strain was measured, however, due to the relatively large proportion of R-phase clearly indicated in Fig. 3. For Treatment B, a comparatively larger residual strain was measured for the tensile test, that was conducted at 19°C (below the A_f for this material), while no appreciable residual strain was measured for the bend test conducted at 24°C (above the A_f for this material).

The success of any predictive engineering methodology depends upon accurate measurement of material behavior. Global measurements, such as far-field load and extension, obtained during uniaxial tensile testing ignore local transformation effects and provide only a limited representation of the material's true behavior. Furthermore, remarkably different behavior can often be observed under different loading scenarios indicating the need for understanding the influence of multidimensional stress states.

Lastly, our results further demonstrate the need to fully consider the differences between the elastic responses of the two material phases [17] in both tension and compression when describing the phase transformation process.

Acknowledgments

The authors would like to gratefully acknowledge the contributions of Randy Lloyd and Nate Stevens from the Idaho National Laboratory and Mark Will at EDM Tek.

References

[1] Miyazaki, S. and Otsuka, K., "Development of shape memory alloys," *ISU International*, Vol. 29(5), 1989, pp. 353–377.

[2] Pelton, A. R., DiCello, J., and Miyazaki, S., "Optimization of Processing and Properties of Medical-Grade Nitinol Wire," in *SMST-2000: Proceedings of the International Conference on Shape Memory and Superelastic Technologies*, S. M. Russell and A. R. Pelton, eds. International Organization on SMST, Pacific Grove, California, 2001, pp. 361–374.

[3] Sczerzenie, F. and Gupta, S., "The Effect of Alloy Formulation on the Phase Transformation Temperature Range of NiTi Shape Memory Alloys," in *Proceedings of the International Conference on Superelastic and Shape Memory Technologies*, 2003, pp. 15–22.

[4] Duerig, T. W. and Zadno, R., Engineering Aspects of Shape Memory Alloys. 1990, pp. 369–383.
[5] Lim, T. J. and McDowell, D. L., "Cyclic Thermodynamic Behavior of a Polycrystalline Pseudoelastic Shape Memory Alloy," *J. Mech. Phys. Solids*, Vol. 50, 2002, pp. 651–676.
[6] Frick, C. P., Ortega, A. M., Tyber, J., Gall, K., and Maier, H. J., "Multiscale Structure and Properties of Cast and Deformation Processed Polycrystalline NiTi Shape-Memory Alloys," *Metall. Mater. Trans. A*, Vol. 35A, 2004, pp. 2013–2025.
[7] Imbeni, V., Mehta, A., Robertson, S. W., Duerig, T. W., Pelton, A. R., and Ritchie, R. O., "On the Mechanical Behavior of Nitinol Under Multiaxial Loading Conditions and in situ Synchrotron x-ray," in *Proceedings of the International Conference on Superelastic and Shape Memory Technologies*, 2003, pp. 267–276.
[8] Post, D., Han, B., and Ifju, P., *High Sensitivity Moiré*. Springer-Verlag, 1994.
[9] Epstein, J. S., Graham, S. M., Perry, Jr., K. E., and Reuter, W. G., "Displacement and Strain Fields for a Bimetallic Strip Under Remote Tension," *ASME J. Appl. Mech.*, Vol. 62, 1995, pp. 997–1004.
[10] Labossiere, P. E. and Perry, K. E., "The Effects of Notches and Grain Size on Transformations in Nitinol," in *Proceedings of the International Conference on Superelastic and Shape Memory Technologies*, 2003.
[11] Perry, K. E. and Labossiere, P. E., "Phase Transformations in Nitinol and Challenges for Numerical Modelling," in *Medical Device Materials II*, ASM International, 2004, pp. 131–134.
[12] Sun, Q-P., Xu, T. T., and Zhang, X., "On Deformation of A-M Interface in Single Crystal Shape Memory Alloys and Some Related Issues," *Trans. ASME, J. Appl. Mech.*, Vol. 121, 1999, pp. 38–43.
[13] Perry, Jr., K. E. and McKelvie, J., "A Comparison of Phase-Shifting and Fourier Methods in the Analysis of Discontinuous Fringe Patterns," *Optics and Lasers in Engineering*, 19(4–5), 1992. (Special issue on fringe analysis).
[14] Deason, V. A. and Ward, M. B., "A Compact Portable Diffraction Moiré Interferometer," in *Laser Interferometry: Quantitative Analysis of Interferograms*, Vol. 1162, SPIE, Bellingham, Washington, 1989, pp. 26–35.
[15] Perry, K. E., Labossiere, P. E., and Steffler, E. D., "Phase Shifted Moiré Interferometry for Accurate Characterization of Superelastic NiTi," in *Proceedings of the Society for Experimental Mechanics 2004 Spring Meeting*. The Society for Experimental Mechanics, 2004.
[16] Kugler, C., Matson, D., and Perry, K. E., "Non-zero Mean Fatigue Test Protocol for NiTi," in *SMST-2000: Proceedings of the International Conference on Shape Memory and Superelastic Technologies*, S. M. Russell and A. R. Pelton eds. International Organization on SMST, Pacific Grove, California, 2001, pp. 409–417.
[17] Liu, Y. and Yang, H., "The Concern of Elasticity in Stress-Induced Martensite Transformation in NiTi," *Mater. Sci. Eng., A*, Vol. A260, pp. 240–245, 1999.